Article

Conformational Heterogeneity of Surface-Grafted Amyloidogenic Fragments of Alpha-Synuclein Dimers Detected by Atomic Force Microscopy

Chad Ray, and Boris B. Akhremitchev

J. Am. Chem. Soc., **2005**, 127 (42), 14739-14744• DOI: 10.1021/ja052932e • Publication Date (Web): 01 October 2005

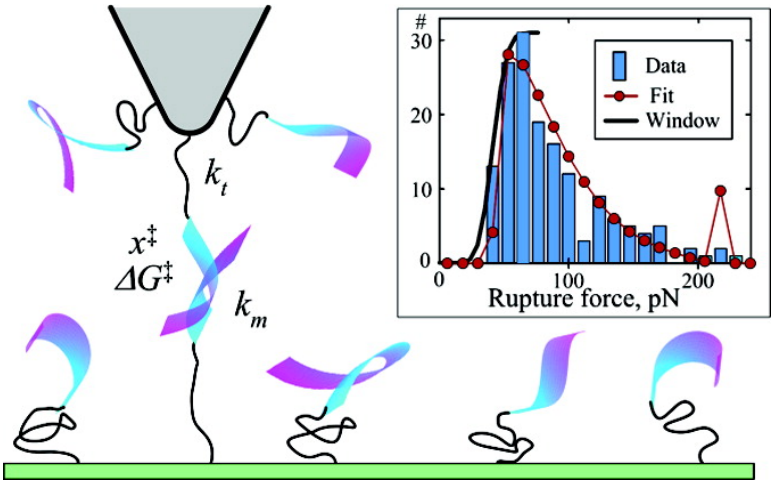

More About This Article

Additional resources and features associated with this article are available within the HTML version:

- Supporting Information
- Links to the 7 articles that cite this article, as of the time of this article download
- Access to high resolution figures
- Links to articles and content related to this article
- Copyright permission to reproduce figures and/or text from this article

View the Full Text HTML

J|A|C|S
ARTICLES
Published on Web 10/01/2005

Conformational Heterogeneity of Surface-Grafted Amyloidogenic Fragments of Alpha-Synuclein Dimers Detected by Atomic Force Microscopy

Chad Ray and Boris B. Akhremitchev

Contribution from the Department of Chemistry, Duke University, Durham, North Carolina 27708

Received May 4, 2005; E-mail: boris.a@duke.edu

Abstract: A force-spectroscopy-based approach is used to characterize separation between amyloidogenic peptide fragments of α-synuclein. Interactions between individual molecules are studied using a scanning-force-microscopy-based technique. α-Synuclein fragments are attached to the solid surfaces via flexible long poly-(ethylene glycol) linkers removing aggregation state uncertainty of solution-based approaches and spurious surface effects. Tethering one fragment to the scanning probe tip and another fragment to the second surface ensures that interactions between tethered molecules are studied. Control experiments with only one tethered peptide indicate peptide−peptide interactions as the source of observed interaction forces in the double-tether experiment. The temperature dependence of rupture forces from 17.5 °C to 40 °C reveals similar molecular parameters indicating that no significant conformational changes occur in the associated molecules over this temperature range. Rate-dependent measurements indicate conformational heterogeneity of joined peptide molecules.

Introduction

There is substantial evidence linking the etiology of neurodegenerative Parkinson's disease (PD) to the fibrillar aggregation of α-synuclein (αS).[1] Small oligomeric species of αS have been implicated in neurotoxicity.[2] Monomeric αS is devoid of a specific secondary structure,[3,4] while fibrillar aggregates have high β-sheet content,[5] indicating that conformational change, a thermally controllable process, occurs at the oligomeric stage. Conformational flexibility of oligomeric species that participate in aggregation may be important to the onset of the amyloid formation.[6] Details of the conformational flexibility of oligomeric species remain unclear.

During aggregation, species of various sizes and conformations are present in solution, making a step-by-step understanding of this process difficult.[7] Studies on an isolated 12 amino acid segment of αS (amino acids 71−82) have demonstrated its propensity to form fibrils on its own and seed the aggregation of wild type (wt) αS, in addition to being solvent inaccessible in wt αS aggregates.[8] Our research design for characterizing the energetics and conformations of specific oligomeric species involves replacing heterogeneous solution conditions with αS segments bound to surfaces.

Force spectroscopy[9,10] is a relatively new technique that analyzes the forces necessary for separating individual bound molecules and quantifies kinetic and thermodynamic parameters of intermolecular interactions that are not available using other techniques.[9−11] Measurements are performed by directional application of separating force between bound molecules. Statistical analysis of measured rupture forces yields the dissociation rate, the height of the energy barrier $\Delta G^{\ddagger}$, and the distance to the transition state $x^{\ddagger}$ in the direction of the applied force. Here interacting molecules are chemically grafted to the flat glass substrate and to the atomic force microscope (AFM) probe via flexible polymeric linkers. Control measurements use samples that include grafted PEG tethers with a capped amino group and without the peptide fragments.

Experimental Section

Materials: Four glass microscope cover slips (Fisher Scientific) and two silicon nitride AFM cantilevers (Veeco, NanoProbe model # NP-S20) are cleaned in piranha solution and then rinsed with 18.2 MΩ water and dried. The AFM cantilevers are immobilized in a custom-made Teflon cantilever holder. All of the modifications are performed

(1) Spillantini, M. G.; Schmidt, M. L.; Lee, V. M. Y.; Trojanowski, J. Q.; Jakes, R.; Goedert, M. *Nature* **1997**, *388*, 839−840.
(2) Conway, K. A.; Lee, S.; Rochet, J.; Ding, T. T.; Williamson, R. E.; Lansbury, P. T. *PNAS* **2000**, *97*, 571−576.
(3) Weinreb, P. H.; Zhen, W.; Poon, A. W.; Conway, K. A.; Lansbury, P. T. *Biochemistry* **1996**, *35*, 13709−13715.
(4) Uversky, V. N.; Li, J.; Fink, A. L. *J. Biol. Chem.* **2001**, *276*, 10737−10744.
(5) El-Agnaf, O. M. A.; Jakes, R.; Curran, M. D.; Middleton, D.; Ingenito, R.; Bianchi, E.; Pessi, A.; Neill, D.; Wallace, A. *FEBS Lett.* **1998**, *440*, 71−75.
(6) Uversky, V. N.; Fink, A. L. *Biochim. Biophys. Acta* **2004**, *1698*, 131−153.
(7) Bernstein, S. L.; Liu, D.; Wyttenbach, T.; Bowers, M. T.; Lee, J. C.; Gray, H. B.; Winkler, J. R. *J. Am. Soc. Mass. Spectom.* **2004**, *15*, 1435−1443.
(8) Giasson, B. I.; Murray, I. V. J.; Trojanowski, J. Q.; Lee, V. M. Y. *J. Biol. Chem.* **2001**, *276*, 2380−2386.
(9) Evans, E.; Ritchie, K. *Biophys. J.* **1997**, *72*, 1541−1555.
(10) Hummer, G.; Szabo, A. *Biophys. J.* **2003**, *85*, 5−15.
(11) Smith, D. A.; Brockwell, D. J.; Zinobar, R. C.; Blake, A. W.; Beddard, G. S.; Olmsted, P. D.; Radford, S. E. *Philos. Trans. R. Soc. London, Ser. A* **2003**, *361*, 713−730.

at room temperature under argon in a glovebox. The first modification is an amination overnight with 30% (mol/mol) 2-aminoethanol-HCl (Aldrich) melted into anhydrous dimethyl sulfoxide (Aldrich) with 0.3 nm molecular sieve beads (Aldrich).[12] The cover slips are submerged in this solution in a glass weigh bottle, held in place using a custom-made Teflon holder. For each of these reactions when the reactions are complete, the cover slips and cantilevers are rinsed in dimethyl sulfoxide (DMSO) (Aldrich) and dimethyl formamide (DMF) (Aldrich). A custom-made Teflon reactor for the cover slips is used for the remaining modification steps to reduce the amount of solution needed. The second modification is activation of the amine for 3 h in a 0.2% (w/v) solution of phenylene diisothiocyanate (Aldrich) in dry DMF.[13] The third modification is PEGylation overnight in 20 mg/mL bis-amine polyethylene glycol (made from 3350 mw PEG) (Aldrich) in dry DMSO.[13] The fourth modification is activation of the free amine on the PEG chain overnight in a 5 mg/mL solution of 3-maleimidobenzoic acid *N*-hydroxysuccinimide ester (Aldrich) in dry DMSO.[13] A 2 mg/mL solution of the αS 12-mer peptide (with added cysteine at C-terminus to aid coupling), (VTGVTAVAQKTVC) (BioPeptide) in dry DMSO is added and reacted overnight.[13] The two samples designated as blanks do not have the peptide added at this step. A 10 mg/mL solution of *N*-hydroxysuccinimide acetoacetate in DMSO is added to block any remaining primary amines.[13] Outside the glovebox the cantilevers and coverslips are put in 50 °C 18.2 MΩ water for 20 min, and then the coverslips are sonicated and cantilevers are shaken (70 rpm on a platform shaker) in toluene, DMF, and ethanol for 5 min each. Finally the coverslips are blown dry with UHP nitrogen (National Welders Supply) and the cantilevers are shaken dry, and both are placed in a vacuum desiccator for 30 min to fully dry the cantilevers. Both are used immediately following this procedure.

Force Spectroscopy: Force spectroscopy measurements were performed using an Asylum Research (Santa Barbara, CA) MFP-3D AFM fitted with a custom-built temperature stage with a modified O-ring that isolates the experimental chamber containing the probe and surface from the environment. The chamber is filled with 210 μL of buffer (pH 7 phosphate buffer, VWR) that the O-ring keeps from evaporating for several days. The interaction between tethered molecules was initiated by bringing two surfaces together. Rupture forces were detected during reverse motion of the probe. Force volume experiments[14] (64 points over 64 lines, 4096 total force measurements per temperature at each of 6 temperatures from 15 °C to 40 °C) are performed over a 25 μm^2 area with a 5 nm relative trigger, a 0.5 s dwell, and a cantilever velocity of 1 μm/s using software written by us (available from Asylum Research). Force−distance curves collected at each probe position were digitally stored for subsequent analysis. The deflection sensitivity is found experimentally using built in functions. The spring constant is found from a thermal noise analysis. Each cantilever is used for the entire series of experiments because the experimental determination of spring constant has ∼20% error.[15] Collection of one force-volume experiment with a 1 Hz repetition rate takes approximately 2.5 h at a given temperature. Before starting the experiments the entire assembled apparatus is allowed to settle for 2−3 h to reduce drift. Upon changing the temperature the apparatus is allowed to equilibrate for 20 min. Temperature change is observed as a significant change in the cantilever deflection signal that remains constant after ∼8 min following a 5 °C temperature change, justifying 20 min equilibration time.

Description of Data Manipulation: Polymer Stretching Model; Cumulative Probability Fitting: Upon collection, force curves are saved as waves in Igor Pro 5 (Wavemetrics Inc., Portland, OR). These waves are exported as ASCII files and processed with a custom program written in Matlab (MathWorks, Inc., Natick, MA). The majority of the collected force curves do not exhibit characteristic separation events. Data processing is automated to remove user bias and speed up the data analysis. The program converts the force curves from deflection versus separation into force versus displacement.

The noise value is calculated as the standard deviation from the off-surface part of the approach line, and the mean noise-value-based threshold is used to detect separation events. A threshold of five standard deviations is applied to the retract curve to detect abrupt transitions in force. After this simple analysis, a filter is applied to remove transitions that occur at separations too close to the surface (<15 nm). A second set of filters refines parameters prior to the freely jointed chain fit to select force events that have a force pattern typical for the separation events coupled to a polymer stretching. Our tests indicate that this initial processing does not eliminate force curves that can be considered for further analysis by a trained user.

The remaining separation events are fit with the extended freely jointed chain model[17] to find the loading rate for each separation event. Force events that are not well fit by the model are eliminated following this step (∼10% of the force curves fit to the polymer stretching model). This model is an extension of the commonly used freely jointed chain (FJC) model. The FJC model predicts extension of the polymer chain $x(F)$ with the Kuhn length l_k and contour length L_c as a function of applied force F according to

$$x(F) = L_c \cdot [\coth(F \cdot l_k / k_B \cdot T) - k_B \cdot T / F \cdot l_k] \quad (1)$$

where k_B is the Boltzman constant and T is the temperature. This equation is usually written as $x(F) = L_c * L(\beta)$ were $L(x)$ is the Langevin function and $\beta = F l_k/(k_B T)$.

Besides an entropic elasticity of the polymer chain included in the FJC model, the extended model includes elongation of the PEG chain due to monomer elasticity as well as conformational transition between helical and planar conformations of the PEG monomers in aqueous solutions.[17] In this model the contour length of stretched polymer consists of the lengths of polymer segments at two different conformations:

$$L_c = N_{planar} \cdot L_{planar} + N_{helical} \cdot L_{helical} \quad (2)$$

Here N_{planar} and $N_{helical}$ are the numbers of segments in planar and helical conformations, respectively. L_{planar} and $L_{helical}$ are the corresponding monomer lengths that are fixed to 3.58 and 2.8 Å, respectively, in our calculations.[17] The contour length defined by eq 2 can be related to the common definition of contour length (the maximum distance between ends of the linear polymer chain) by noting that if $N_{helical}$ and N_{planar} have fixed (force-independent) values, then the usual definition of contour length can be applied. The ratio of $N_{helical}$ to N_{planar} depends on the applied force according to

$$\frac{N_{helical}}{N_{planar}} = \exp(\Delta G(F)/k_B \cdot T) \quad (3a)$$

$$\Delta G(F) = \Delta G_0 - F \cdot (L_{planar} - L_{helical}) \quad (3b)$$

Here $\Delta G(F)$ is the force-dependent free energy difference between the two states, and ΔG_0 is this difference at zero applied load that is fixed to 7.48 kJ/mol in our calculations.[17] Combining eqs 1, 2, and 3 together gives the extension of PEG chain with N monomers:

(12) Hinterdorfer, P.; Gruber, H.; Kienberger, F.; Kada, G.; Riener, C.; Borken, C.; Schindler, H. *Colloids Surf., B* **2002**, *23*, 115−123.
(13) Hermanson, G. *Bioconjugate Techniques*; Academic Press: New York, 1996.
(14) Laney, D. E.; Garcia, R. A.; Parsons, S. M.; Hansma, H. G. *Biophys. J.* **1997**, *72*, 806−813.
(15) Proksch, R.; Schäffer, T. E.; Cleveland, J. P.; Callahan, R. C.; Viani, M. B. *Nanotechnology* **2004**, *15*, 1344−1350.
(16) Ratto, T. V.; Langry, K. C.; Rudd, R. E.; Balhorn, R. L.; Allen, M. J.; McElfresh, M. W. *Biophys. J.* **2004**, *86*, 2430−2437.
(17) Oesterhelt, F.; Rief, M.; Gaub, H. E. *New J. Phys.* **1999**, *1*, 6.1−6.11.

$$x(F) = N\cdot\left(\frac{L_{\text{planar}}}{\exp(-\Delta G/k_B\cdot T)+1} + \frac{L_{\text{helical}}}{\exp(+\Delta G/k_B\cdot T)+1}\right)\cdot [\coth(\beta) - 1/\beta] + N\cdot\frac{F}{K_s} \quad (4)$$

Here the segmental elasticity K_s provides the chain extension at high loads and is held at 150 N/m.[17] This model was used to fit the force curves with two free parameters: the number of monomers in the chain and the Kuhn length. The Kuhn length was allowed to vary to obtain a close fit to the data near the separation point. It was noted that when both FJC and extended FJC models were used to fit the experimental data, the FJC model produced systematically higher tether elasticity values as shown in Figure 1. The error in tether elasticity will propagate in the error in the loading rate *lr* that is calculated according to $lr = v(k_t^{-1} + k_c^{-1})^{-1}$, where k_c is the spring constant of the cantilever, k_t is the spring constant of the tether, and v is the velocity of the cantilever base. The extended FJC model fits the stretching curve closely, providing a more accurate loading rate determination.

Kinetic parameters characterizing the separation between individual molecules were obtained from rupture forces and loading rates by using the Hummer−Szabo model from ref 10. According to this model, the cumulative probability to rupture at forces below F_0 is calculated from the survival probability $S(t)$ according to

$$P(F < F_0) = 1 - S\left(\frac{F_0 + \kappa_s\cdot x^{\ddagger}}{\kappa_s v}\right) \quad (5)$$

Here κ_s is the combined stiffness of the polymeric tether and the cantilever, v is the velocity of the cantilever's base, and $x^{\ddagger}$ is the distance to the transition state as illustrated in Figure 2 that shows the free energy surface used in the model.

This model considers separation from the binding harmonic potential with a sharp cusp that corresponds to the transition state. Separation is driven via spring with string constant k_s that moves with constant velocity v. At long times the mean pulling coordinate x becomes

$$\bar{x}(t) = t\cdot v\frac{k_s}{k_s + k_m} \quad (6)$$

where k_m is the molecular spring constant. The survival probability at time t is given by

$$S(t) = \exp\left[-\frac{K_0\cdot\exp(-\beta\cdot\kappa_s\cdot(x^{\ddagger})^2/2)}{\beta\cdot\kappa_s\cdot v\cdot x^{\ddagger}\cdot(\kappa_m/\kappa)^{3/2}}\cdot(\exp(\beta\cdot\kappa_s\cdot v\cdot x^{\ddagger}\cdot t) - (\beta\cdot(\kappa_s\cdot v\cdot t)^2)/2\cdot\kappa - 1)\right] \quad (7)$$

with

$$\kappa = \kappa_m + \kappa_s$$

$$\beta = (k_B\cdot T)^{-1}$$

Here K_0 is the intrinsic rate constant. Separation occurs prior to time τ when extension reaches $x^{\ddagger}$; at this point the survival probability is set to zero. This gives the maximum force with nonzero survival probability $F_{max} = k_m x^{\ddagger}$. The mean force during the pulling experiment is calculated according to

$$\bar{F} = -\kappa_s[x^{\ddagger} - v\cdot\int_0^{\tau} S(t)\cdot dt] \quad (8)$$

Equations 5 and 7 are used to calculate the cumulative rupture probability for experimental values of rupture force F, loading spring constant k_s, probe velocity v, and temperature T with given values of $x^{\ddagger}$, $\Delta G^{\ddagger}$, and K_0. Equation 8 is used to calculate the expected mean force dependence on the loading rate.

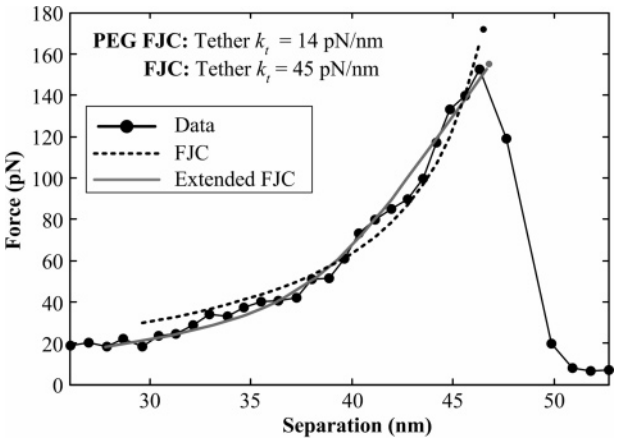

Figure 1. A typical force event is fitted with both the FJC model (dashed line) and the extended FJC model (solid line).

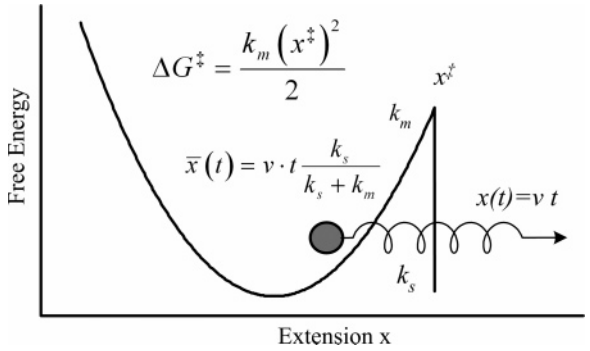

Figure 2. Free energy surface in the forced rupture model.[10]

Experimental values of rupture forces are binned into histograms $H_F(F_i < F < F_{i+1})$, and the mean value of force is calculated for each histogram bin to be used in further analysis as the rupture force. The number of events in each histogram bin is used to obtain the cumulative rupture probability as

$$P_{ex}(F < F_i) = \frac{\sum_{j=1}^{i} H_F(F_j)}{\sum_{j=1}^{N_B} H_F(F_j)} \quad (9)$$

where N_B is the number of histogram bins and $H_F(F)$ is the number of force values averaged in each bin. It has to be noted that if, due to limited force sensitivity, events at low rupture force were not registered, the cumulative probability calculated according to eq 9 will have an associated error even at larger forces. Introducing the error function as described below solves this problem. Cumulative probability given by eq 5 is calculated for a fixed value of k_s, while the experiment results in a distribution of these values. Expected cumulative probabilities can be calculated for each k_s value and the results can be averaged to obtain the expected probability. We noted that calculation of the cumulative probability distribution for each k_s value can be replaced by binning k_s values into several bins and average several resulting distributions with weights corresponding to the number of particular k_s values in each bin. Thus, the expected cumulative probability distribution is calculated according to

$$P(F < F_i) = \frac{H_{ks}(ks_j) \cdot P(F < F_i, ks_j)}{\sum_{j=1}^{N_{ks}} H_{ks}(ks_j)} \quad (10)$$

where $H_{ks}(k_s)$ is the number of k_s values in each bin of the k_s histogram and N_{ks} is the number of histogram bins.

Since the rupture events at low forces might escape detection due to deflection signal noise, a window function that indicates the force sensitivity was used in the data analysis. For example if all the rupture events below 40 pN were ignored, true probability distribution will be significantly modified as shown in Figure 3.

Therefore, prior to calculating the fit error, the expected distributions were adjusted to include this effect. The actual window function used in calculations was selected to match the initial part of the force histogram as shown in the insert in Figure 6. This shape makes certain assumptions about the shape of the expected probability distribution at the rising edge. Therefore, during the fit procedure, calculated errors were weighted by the same window function to give larger weight to errors corresponding to forces above the window edge.

The parameters fit was performed in Matlab minimizing the RMS fit error. Systematic variation of the rupture force values in the ±20% range was performed to estimate influence of systematic error in the force measurements on fit parameters. This variation results in approximately ±25% variation in the molecular spring constant k_m, (−5%, −20%) variation in the intrinsic rate constant K_0, (+8%, −20%) changes in fitted barrier widths $x^‡$ and surprisingly only (−1.5%, 0.5%) variation in the barrier heights $\Delta G^‡$. Systematic variations in k_s values indicated that the most influenced fit parameter is K_0 that changes by the same relative amount as k_s and change in other parameters was insignificant (few percent for ±33% k_s change). Large random error of the fit is associated with the shallowness of the error function as shown Figure 4.

Results and Discussion

The double-tether approach[16] is used to distinguish the rupture events between the tethered molecules from the ruptures between the tethered molecule and the substrate surface. Force−distance curves reveal that individual single molecule rupture events occur at different probe positions above the sample surface. Prior to rupture events, the polymer tethers are stretched with end-to-end distances far exceeding the average distances found at thermal equilibrium. This stretching results in a characteristic force-separation dependence (shown in Figure 1) that is used as an initial selection criterion in data analysis. Mass spectroscopy of PEG linkers reveals a molecular weight distribution from 3200 to 4100 Da at half-maximum (see Figure 5 for a mass spectrograph). Therefore, long tethers are used to clearly identify rupture events between tethered peptides. Rupture events that correspond to the sum of the tether's stretched lengths (ranging from 40 to 75 nm) were used in the statistical analysis of rupture forces. The indicated range includes the polydispersity of tethers as well as conformational transition of PEG tethers under force.[17] Force−distance curves with multiple rupture events, an indication that the measured interactions may not be single molecular in nature, are also eliminated during this step to ensure that every rupture event used in the statistical analysis is the interaction of one molecule from the surface and one molecule from the AFM tip.

To attribute measured forces to interactions between tethered peptides, test experiments were performed that included rupture force measurements between peptides tethered via PEG linkers to the probe and the surface equipped with an acetoacetate

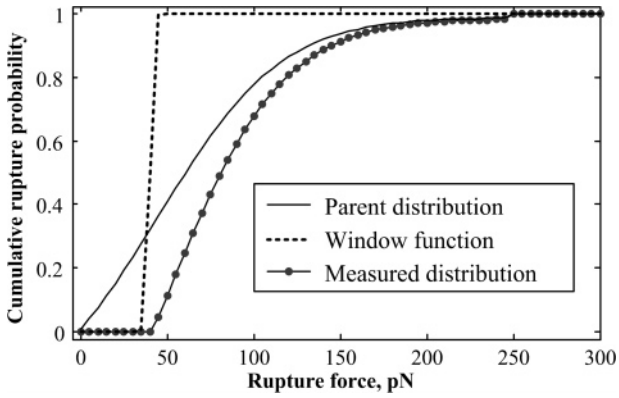

Figure 3. Figure shows effect of limited force sensitivity on measured cumulative rupture probability.

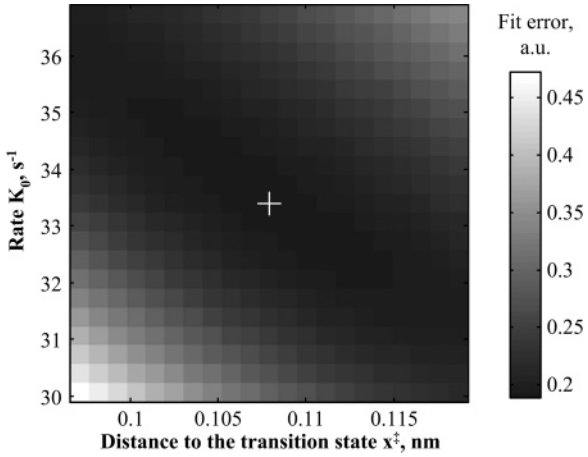

Figure 4. Fit error function dependence on parameters K_0 and $x^‡$ that were varied independently and at fixed $\Delta G^‡$ value. Cross mark in the image indicates minimum of the error function.

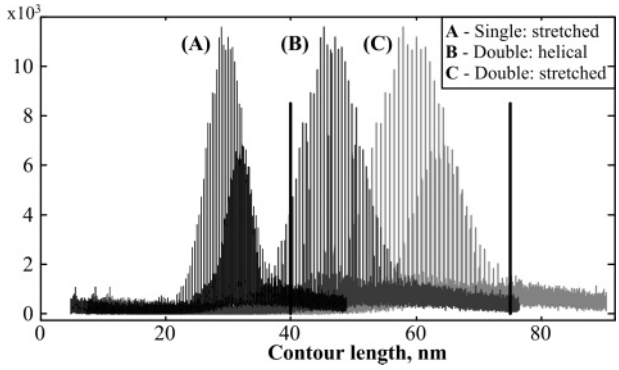

Figure 5. (A) Single stretched PEG chain contour lengths. (B) Double tether helical PEG contour length. (C) Double tether stretched PEG contour length. Experimentally the contour length can be anywhere between these bounds, delineated by the vertical bars, explaining the distribution of separation values.

capped PEG linker. These measurements show a minor fraction of polymer stretching events (0.18% of all approaches) at a separation corresponding to a double-linker length in comparison to ∼2% probability when both tethers are equipped with peptides. This indicates that typical rupture events detected between surfaces with tethered peptides arise from peptide−peptide interaction and not from peptide−linker interaction.

An extended freely jointed chain (FJC) model that includes a conformational transition of PEG linkers[17] was fit to each

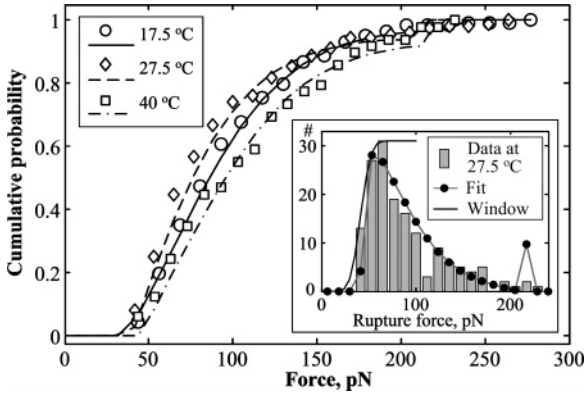

Figure 6. Measured cumulative distributions of rupture forces at different temperatures as symbols with stochastic model fit lines. The insert shows the histogram of rupture forces at 27.5 °C, the fit derived from the cumulative probability, as well as the force cutoff function that results from the limited force sensitivity.

Table 1. Stochastic Model Parameters Used to Fit Data in Figure 6

temp, °C	K_0, 1/s	$\Delta G^{\ddagger}$, kJ/mol	$x^{\ddagger}$, nm	k_m, N/m
17.5	33 ± 15	16 ± 4	0.11 ± 0.06	2.1 ± 1.3
27.5	64 ± 7	12 ± 3	0.10 ± 0.03	2.1 ± 0.8
40	28 ± 12	17 ± 4	0.12 ± 0.04	1.9 ± 0.8

tether-stretching event. The Experimental Section includes further details of the fit procedure.

Fit parameters and rupture force were used to calculate the tether spring constant at the rupture, k_t. A stochastic model[10] successfully used by others[18,19] was used to fit cumulative probabilities of rupture forces that were collected at different temperatures. This model calculates the cumulative probability distribution of rupture forces for a given set of experimental parameters (temperature T, loading spring constant k_s, velocity of the probe's base υ) and a set of fit parameters (the dissociation rate K_0, the height of the energy barrier $\Delta G^{\ddagger}$, and the distance to the transition state $x^{\ddagger}$). The overall loading spring constant is calculated according to $k_s = (k_t^{-1} + k_c^{-1})^{-1}$ where k_c is the spring constant of the cantilever and k_t is the spring constant of the tether. Measured k_s values were binned in a histogram, and for each k_s bin, the cumulative probability distribution was calculated. The resulting distribution was constructed by adding individual distributions with weights that correspond to the frequency of occurrence of a particular k_s value. Figure 6 shows the measured cumulative distributions of rupture forces with fit lines superimposed in the graphs. Different lines and symbols correspond to measurements at different temperatures. These measurements address known temperature effects on fibrillation.[4]

Limited force sensitivity is accounted for in the model by a window function that matches the rising edge of the histogram as indicated in the insert in Figure 6.[20] Table 1 lists the fit parameters where the stiffness of intermolecular potential $k_m = 2\ \Delta G^{\ddagger}/(x^{\ddagger})^2$ is also indicated. Barrier heights reported here are similar to the barrier heights of titin unfolding.[10] The parameters' errors were estimated from the covariance matrix. This calculation underestimates errors for dependent fit parameters.[21]

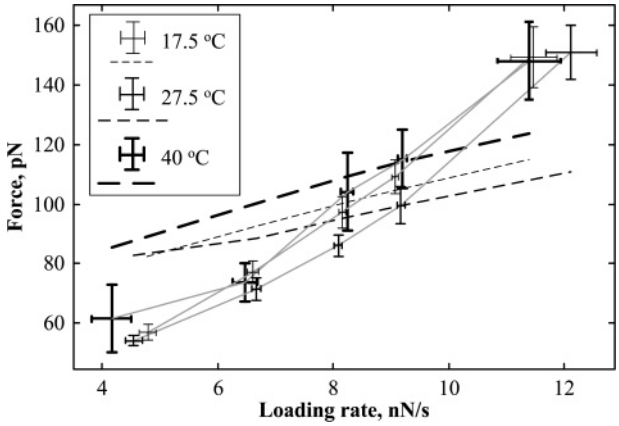

Figure 7. Figure shows measured rupture force vs loading rate dependence (error bar symbols) and the same dependence calculated using distribution fit parameters as those in Figure 6 (dashed lines).

It has to be noted that the fit error dependence on rate K_0 is very shallow resulting in large error in the rate estimates. Although this model fits experimental distributions reasonably well, it fails to predict force vs loading rate dependence. As noted in ref 10, at high loading rates rupture force becomes proportional to the square root of the loading rate. Experimental data show much a steeper dependence with a log−log slope approximately equal to 1, as shown in Figure 7.

The measured slope is unattainable in this stochastic model and indicates that separation occurs from more than one state with separate states having different thermodynamic and kinetic parameters. We note that separation from these different states should occur at different subsets of the loading rates; only this can result in the steep loading rate dependence. In addition, statistical analysis of experimental data indicates no significant correlation (0.04) between measured loading rates and the tip−sample separation at rupture. This observation indicates that the states implicated above are not sequential states connected by some rate process but rather independent conformations in a heterogeneous sample.

We note here that the high loading rate dependence of rupture forces that is seen in Figure 7 signifies that temperature dependences of the rupture forces should be considered in conjunction with the rate dependences because slightly different statistics in loading rate at different temperatures might be misinterpreted as temperature-dependent changes.

Summary

Our data indicate that αS fragments form conformationally heterogeneous dimer states. The experimental technique is based on a double tether[16] force spectroscopy approach. This approach identifies the force events of interest, namely separate interactions between individual tethered molecules from interactions with the substrate or molecules directly bound to the substrate. Test experiments where one tether is not equipped with the peptide demonstrate that the interactions studied arose from peptide−peptide interactions as opposed to peptide−tether or peptide−surface interactions. An extended freely jointed chain model[17] that includes force-driven conformational transition of

(18) Meadows, P. Y.; Walker, G. C. *Langmuir* **2005**, *21*, 4096−4107.
(19) Weiland, J. A.; Gewirth, A. A.; Leckband, D. E. *J. Phys. Chem. B.* **2005**, *109*, 5985−5993.
(20) Friedsam, C.; Wehle, A. K.; Kühner, F.; Gaub, H. E. *J. Phys.: Condens. Matter* **2003**, *15*, S1709−S1723.
(21) Bevington, P. R.; Robinson, D. K. *Data reduction and error analysis for the physical sciences*; McGraw-Hill: New York, 1992.

the PEG tethers was used to fit experimental force events and to calculate the loading spring constant for use in creating the cumulative probability of rupture distributions. The resulting distributions were corrected for the limited low force sensitivity using an estimated window function.[20] Corrected distributions were well fit by a forced rupture model,[10] but the reapplication of the fit parameters to the model resulted in a force-loading rate dependence which deviated from the experimental data. The inability of the model to fit this dependence indicates that the experimental data contains more than one independent state, i.e., it contains a heterogeneous mixture of states that have different force-loading rate dependences. This result is supported by the literature as recent measurements have indicated that a similar section of αS (amino acids 74−94) resides mostly in two conformations of extended or intermediate length.[22] In addition mass-spectrometric studies show conformational heterogeneity of αS dimers.[7] Our data indicate that the conformational variability persists in the dimer state of αS fragments. Future research will clarify if this conformational heterogeneity persists for longer fragments and if this heterogeneity can be controlled by inclusion in the sequence of amino acids with charged side chains.

Acknowledgment. The authors thank Duke University and the Camille and Henry Dreyfus Foundation for financial support plus Chao Gu and George Dubay for MALDI-MS spectra.

JA052932E

(22) Lee, J. C.; Langen, R.; Hummel, P. A.; Grey, H. B.; Winkler, J. R. *PNAS* **2004**, *101*, 16466−16471.